Chall. Nano Micro Scale Sci. Tech., 9(2):135-150, Summer and Autumn 2021
DOI: 10.22111/CNMST.2021.37182.1203

ORIGINAL RESEARCH PAPER

MHD Three-Dimensional Flow of Couple Stress Nanofluids Over a Stretching hseet Through a Porous Medium in Presence of Heat Generation/Absorption and Non-Linear Thermal Radiation

R. A. Mohamed [1], S. E. Ahmed [1, 2], A. M. Aly [1, 2], S. M. Abo-Dahab [1, 3] and M. S. Soliman [1]

[1] *Department of Mathematics, Faculty of Science, South Valley University, Qena, Egypt.*
[2] *Department of Mathematics, Faculty of Science, Abha, King Khalid University, Saudi Arabia.*
[3] *Computer Science Department, Faculty of Computers and Information, Luxor University, Luxor, Egypt*

Received 9 January 2021; revised 19 October 2021; accepted 24 October 2021;

ABSTRACT: This article is concerned with study of the steady and incompressible three-dimensional flow of magnetohydrodynamic couple stress nanofluids over a stretching sheet through a porous medium under influence of, non-linear thermal radiation and heat generation/absorption, taking into account effects of both Brownian motion coefficient and thermophoresis coefficient. On the other hand, the system of nonlinear partial differential equations governing the flow process has been transformed into a system of nonlinear ordinary differential equations using similarity transformations and dimensionless variables, knowing that the numerical method used to solve the new system of differential equations is the fourth-order Runge-Kutta method with the shooting technique in the code of MATLAB program. The effects of all physical parameters resulting from this study on the distributions of velocity, temperature and concentration of nanoparticles within the base fluid were studied by means of graphs that were made by the MATLAB program. Finally, some of the results of the current study showed that the effects of the magnetic field parameter and Darcy number on the velocity distribution were negative, while their effect on the concentration of nanoparticle distribution was positive.

KEYWORDS*: Couple stress fluid, Nanofluid, Thermal radiation, Magnetohydrodynamic (MHD), Porous media.*

INTRODUCTION

Researchers in the field of fluid properties around the world are making every effort to study the problems of non-Newtonian fluid flow, and the reason behind this is the tremendous progress in technological applications resulting from the study of this type of fluid at the present time. Non-Newtonian fluids are one of the types of fluids that are characterized by viscosity, as they are thick fluids in which viscosity changes according to the change in pressure and temperature, examples of these fluids, nature extrusion of polymer fluids, drilling mud, suspension solutions, cosmetic and food products, solidification of liquid crystals, cooling of metallic plates in a bath, exotic lubricants, also ketchup, toothpaste, blood, paints colloidal and many others. Couple Stress fluid theory is one of the most important theories that have attracted the attention of many researchers in the field of non-Newtonian fluid flow studies, it has got the special status because of the spin field in the fluid which sets up an anti-symmetric stress, known as couple stresses. Stokes [1] was the first to develop the fundamental theory and constituent rates of a double stress fluid model, the most important characteristic of this theory is that it links the couple pressures with the classical Cauchy pressures. On the other hand, the couple stress fluid contains randomly inelas-tic particles inside a viscous medium.Examples of couple stress fluids are blood, liquid crystals, colloidal fluids, lubrications and additive electro-rheological fluids etc. Devakar et al. [2] studied analytical solutions of couple stress fluid flows with slip boundary conditions. Zhang and Chen [3] investigated dielectrophoretic microfluidic device for separation of red blood cells and platelets: a model-based study. Zhang and Chen [4] analyzed blood cells separation microfluidic chip based on dielectrophoretic force. Han and Chen [5] discussed new insights into the pressure during the merged droplet formation in the squeezing time. There are also many studies of couple stress fluid flow with different geometries see [6 – 9]. Study of nanofluids has received a critical interest in recent years among researchers in the field of hydrodynamic around the world because this type of fluid has important applications and uses in most aspects of life and the first to discover this type of fluid is Choi [10] and nanofluids is the most recent chapters of fluids as it contains inside them on very fine metallic particles measured at the nanometer scale and these particles have a high thermal conductivity as well as have engineering and medical applications and the researchers in the field of nanofluids are trying to take advantage of the thermal conductivity feature in the development of thermal conduction fluids. Waqas et al. [11] illustrated significance of magnetic field and activation microorganisms. Waseem et al. [12] studied

*Corresponding Author Email: *m.soliman757@yahoo.com*
Note. This manuscript was submitted on January 9, 2021; approved on October 19.

gravity-driven hydromagnetic flow of couple stress hybrid nanofluid with homogenous-heterogeneous reactions. Afzal et al. [13] performed thermal and concentration convection in nanofluids for peristaltic flow of magneto couple stress fluid in a nonuniform channel. Usman et al. [14] explained electromagnetic couple stress film flow of hybrid nanofluid unsteady rotating disc. Narayana et al. [15] presented numerical simulation of nonlinear thermal radiation on the 3D flow of a couple stress Casson nanofluid due to a stretching sheet. The studies referred by [16 - 22] include different models of non-Newtonian nanofluids with different geometries.

The process of fluid flow influenced by a magnetic field is a physical phenomenon called magnetohydrodynamic, which is symbolized by MHD, on the other hand can be defined as the study of the magnetic properties and behavior of electrically conducting fluids. Examples of such magnetofluids include plasmas, liquid metals, salt water, and electrolytes. The word (magnetohydrodynamics) is derived from magneto meaning magnetic field, hydro meaning water, and dynamics meaning movement and who the first to start studying this field is Alfvén [23] in 1942. On the other hand, the process of thermal radiation is the temperature emitted by hot objects like that thermal radiation emitted from incandescent light bulb emitting visible-light, infrared radiation emitted by a common household radiator or electric heater, as well as radiation from hot gas in outer space. A person near a raging bonfire feels the radiated energy of the fire, even if the surrounding air is very cold. Thermal radiation is generated when thermal energy is converted to electromagnetic radiation by the movement of the charges of electrons and protons in the material. Mabood et al. [24] debated features of entropy optimization on MHD couple stress nanofluid slip flow with melting heat transfer and nonlinear thermal radiation. Ahmed et al. [25] explained energy on the features of stratified mixed radiative-convective couple-stress nanofluid flows with motile over an

magnetohydrodynamic Maxwell nanofluid flow over a stretching surface through a porous medium effects of nonlinear thermal radiation convective boundary conditions and heat generation/ absorption. Mohamed et al. [26] studied MHD Jeffrey nanofluid flow over a stretching sheet through a porous medium in the presence of nonlinear thermal radiation and heat generation/absorption. Mohamed et al. [27] investigated MHD Casson nanofluid flow over a stretching surface embedded in a porous medium effect of thermal radiation and slop conditions. Bouslimi et al. [28] analyzed MHD Williamson nanofluid flow over a stretching sheet through a porous medium under effects of Joule heating, nonlinear thermal radiation, heat generation/absorption and chemical reaction. references [29-32] refers to studying the magnetohydrodynamic flow of non-Newtonian nanofluid with different geometries. Changdar and Soumen [33] studied analytical solution of mathematical model of magnetohydrodynamic blood nanofluid flowing through an inclined multiple stenosed arteries, also that Sedighi [34] investigated steady boundary layer magnetohydrodynamic viscous flow and heat transfer of nanofluid over stretching sheet in presence of radiation and heat source, while Ashikin et al. [35] analyzed rotating flow over a shrinking sheet in nanofluid by using Buongiorno model and thermophysical properties of nanoliquid. Entropy generation due to MHD mixed convection of nanofluid between two concentric cylinders with radiation and joule heating effects presented Srinivasacharya and Shafeeurrahman [36]. Borty et al. [27] performed analytical approach to a Jeffrey nanofluid flow towards a stagnation point coexisting with magnetic field and melting heat effects, and Raju et al. [38] provided a free convective heat transfer of MHD Cu- kerosene nanofluid with temperature dependent viscosity, on the other side, Jalilpour et al. [39] presented the MHD non-orthogonal stagnation point flow of a nanofluid towards a stretching surface in the presence of thermal radiation.

In fluid dynamics, fluid flow through a porous medium is defined as the flow of fluid through the pores or voids in this medium such as sponge, wood, or sand that is used in the water purification process, and the fluid flow through a porous medium help on store some of the fluid mass in the pores in this medium. Imtiaza et al. [40] excogitated flow of magneto nanofluid by a radiative exponentially stretching surface with dissipation effect. Awais et al. [41] examined the hydromagnetic couple-stress nanofluid flow over a moving convective wall: OHAM analysis. Muhammad et al. [42] investigated the squeezed flow of a nanofluid with Cattaneo–Christov heat and mass fluxes. Khan et al. [43] presented Brownian motion and thermophoresis effects on MHD mixed convective thin film second-grade nanofluid flow with hall Effect and heat transfer past a stretching sheet. Reddy et al. [44] investigated temperature-dependent viscosity and second order slip flow on MHD casson radiative nanofluid over stretching sheet. Hussain et al. [45] studied radiative magneto-nanofluid over an accelerated moving ramped temperature plate with hall effects. Naramgari and Sulochana et al. [46] take a study the MHD flow of dusty nanofluid over a stretching surface with volume fraction of dust particles. Mahanthesha et al. [47] reviewed a study of nonlinear radiative heat transfer in MHD three-dimensional flow of water based nanofluid over a non-linearly stretching sheet with convective boundary condition. Kumar et al. [48] analyzed hydro magnetic boundary layer slip flow of nanofluid through porous medium over a slandering stretching sheet. Hayat et al. [49] studied magnetohydrodynamic three-dimensional flow of viscoelastic nanofluid in presence of nonlinear thermal radiation. New features on MHD have been discussed considering external forces and parameters [50-52]. Kandasamy at al. [53] investigated thermophoresis and Brownian motion effects on MHD boundary-layer flow of a Nanofluid in the presence of thermal stratification due to solar radiation. Ramesh at al. [54] examined MHD flow of Maxwell fluid over a stretching sheet in the presence of nanoparticles, thermal radiation and chemical reaction.

The main objectives of this research are to study the three-dimensional flow of electromagnetic couple stress nanofluids on a stretching surface through a porous medium taking into account the study of the effect of non-linear heat radiation and the heat generation/absorption on the distributions of velocity, temperature and concentration of nanoparticles in addition to the effects of Brownian motion coefficient and thermophoresis coefficient, by making graphs and numerical tables. On the other hand, the system of non-linear partial differential equations was transformed into a system of ordinary differential equations using the appropriate transformations and was numerically resolved using the fourth order Runge/Kutta method and the effects of all physical parameters were studied as previously using graphs and numerical tables.

FORMULATION OF THE PROBLEM

In the current study, the steady and incompressible flow of the magnetohydrodynamic couple stress nanofluid was considered a three-dimensional flow over a regular stretching surface through a suitable porous medium, Cartesian coordinates were selected to describe this study whereas affects the movement of this fluid a fixed magnetic field in the direction of the $z-$ axis (perpendicular to the direction of the fluid movement) with the knowledge that the induced magnetic field It was neglected because Reynolds's number was very small while the study is supported by new effects such as non-linear thermal radiation and heat generation/absorption coefficients. It was adopted the Cartesian coordinate system in such a way that x – axes, $y-$ axes are in the direction of motion and $z-$ axes is normal to the sheet. The sheet at $z=0$ is stretched in $x-$ and $y-$ directions with velocities $U_w(x)$ and $V_w(y)$ respectively see Figure (1a). The governing boundary layer equations in the present flow is giving as follows:

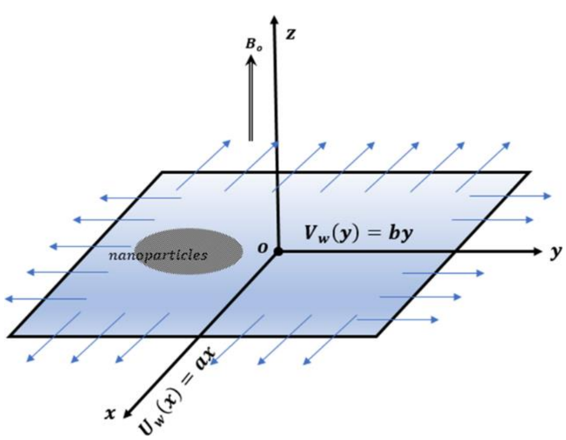

Fig. 1a. Effect of the magnetic field *M* on the velocity profile.

Ding et al. [19] investigated heat transfer behavior of multi-walled carbon nanotubes (MWCNT) by flowing them in a horizontal tube. Their studies remarked that the concentration of CNT and the Reynolds number made good contribution to the heat transfer augmentation. Their results clearly indicate that CNTs having 0.5 wt% and at Reynolds number of 800, a maximum enhancement of 350% is achieved. Chen et al. [20] conducted a series of experimental studies to predict heat transfer coefficients and investigate the behavior of titanium nanotubes. They also performed some experiments to explore various factors, including effective thermal conductivity, forced convective heat transfer, and rheological behavior of nanofluids. Only a maximum of 5% enhancement was observed by the titanate nanofluids under particle loading of 2.5 wt%. Kayhani et al. [21] examined the pressure drop and heat transfer in a turbulent flow of the aqueous solution of TiO_2 nanoparticels, which flowed in a constantly heated horizontal circular tube containing 0.1, 0.5, 1.0, 1.5 and 2.0% volume concentrations of nanoparticles. The results showed an increase in heat transfer coefficient as a result of increased nanofluid volume fraction. The Nusselt number was also found increased to be about 8% for nanofluid at a Reynolds number of 11800, with 2.0% nanoparticles volume fraction. Heat transfer coefficient and friction factor with SiO_2/water nanofluid up to 4% particle volume concentration were determined by Azmi et al. [22].

At a volumetric concentration of 3%, they saw an increasing and then a decreasing trend in heat transfer coefficients.

At this volumetric concentration, the maximum increase in the Nusselt number was approximately 38% within the Reynolds range. Esfe and Saedodin [23] conducted a series of experimental studies on dynamic viscosity, Nusselt number, and thermal conductivity of turbulent forced convection of MgO-water nanofluids flowing in a circular tube. The pure water and nanofluid with the nanoparticle volume fraction of 0.005, 0.01, 0.015, and 0.02 and the nanoparticles diameter of 20,40,50 and 60 nm were considered. Experimental results showed a tendency of heat transfer to increase due to the presence of nanoparticles in pure water. Ali [24] experimentally tested the internal convective heat transfer of SiO_2-water nanofluids flowing in a copper tube for a fully turbulent regime. He also determined the local convective heat transfer coefficient in different positions along the pipe in different Reynolds numbers. The maximum increase was 8-9% at 0.001 vol% SiO_2 nanoparticles. However, convective heat transfer coefficient increased by 27% at 0.007 vol% SiO_2 nanoparticles. Abdolbaqi et al [25] studied the forced convection heat transfer of CuO, TiO_2 and Al_2O_3 under turbulent flow through a straight square. The boundary conditions were applied under a 5000 W/m^2 heat flux, the Reynolds number 10^4-10^6, and a constant volume concentration of 1 to 4%.

The results suggested an increase in heat transfer and wall shear stress with increasing nanofluid volume concentration. CuO nanofluids appear to increase heat transfer significantly. The study remarked the enhancement of the friction factor and the Nusselt number is 2% and 21%, respectively, for the channel at all Reynolds numbers. Hemmat Esfe [26] et al. reported results of experiments on thermal conductivity, viscosity and turbulent heat transfer behavior of MgO–water nanofluid in a straight circular tube for the volume fraction of nanoparticles <1%. They observed that most of the conventional models fail to predict the thermal conductivity and dynamic viscosity of the MgO–water nanofluid accurately.

Their results indicated that addition of low value of nanoparticles to the base fluid results in enhanced heat transfer. As observed in the literature review, the heat transfer properties of MgO nanoparticles have been less studied than those of other metal oxide nanoparticles (e.g., Al_2O_3, TiO_2, and CuO). On the other hand, lack statistical analysis exists on the operating parameter. The majority of researchers indicated that nanoparticle concentration, temperature, and nanofluid flow rate (Reynolds number) affect heat transfer coefficient. Nevertheless, nothing could be understood by comparing the operational parameters. The present study includes an experimental study of the convective heat transfer of MgO-water nanofluids, which passes through a copper tube in a fully turbulent regime under constant heat flux conditions. Nusselt number and convective heat transfer coefficient were investigated in a very dilute concentration of nanoparticles. Local convective heat transfer coefficient was also observed at various points along the pipe. The main objectives of this study are three-fold: 1) to assess the impact of each parameter on the Nusselt number and local heat transfer coefficient and 2) to apply the statistical Taguchi experimental design method on the optimization of factors and to find a combination of parameters to achieve the maximum value of the Nusselt number and 3) to examine all the interaction effects of factors.

PREPARATION OF THE NANOFLUID

MgO nanoparticles with distilled water (as a base fluid) are used in this work. Nanoparticles are manufactured by the US Nanomaterials Research Company, USA. The specifications of the nanoparticles are shown in Table 1. Here, a transmission electron microscope (TEM) has been used to approximate the shape and size of MgO nanoparticles.

Table1

Specification of nanoparticle used in this study

Nanoparticle	Magnesium Oxide (MgO)
Average particle size (nm)	20
Purity	>98%
Density (kg/m^3)	3580
Color	white
Morphology	nearly spherical
Specific area(m^2/g)	>60
Specific heat (J/kgK)	880
Thermal conductivity (W/mK)	45

Figure 1 demonstrates that the shape and size of nanoparticles are approximately spherical and around 20nm, respectively. Many researchers employ this method [27-28].

There are two methods, i.e., single-step and two-step, for nanofluid production. Providing stable nanofluid is a challenge. Various methods are used to achieve stable nanofluid, including changes in nanofluid pH, the addition of surfactants, and ultrasonic vibration. In this study, nanofluid was prepared with a concentration of 0.05 and 0.15 of vol%. A specific amount of MgO nanoparticles is weighed (accurate to three decimal places) to which distilled water was added as a base fluid. After one hour of mixing with a magnetic stirrer, the nanofluid was put in a ultrasonic vibrator (BANDELIN Company with a power = 240 kW and frequency = 35 kHz) for 5 hours. This procedure is utilized to create a stable suspension system of nanofluid and break the agglomeration of nanoparticles in fluid. The prepared solution remains stable at static condition for 3 day after experimentation. No surfactant was utilized in the study as it may have affected the thermal conductivity of nanofluids [29-30]. Repeatability was assessed during the experiments. Some experiments were randomly repeated at various points in times, revealing a slight difference between the two. That is, over time, there has been no change in test results, indicating nanofluid stability.

$$\frac{\partial u}{\partial x}+\frac{\partial v}{\partial y}+\frac{\partial w}{\partial z}=0, \tag{1}$$

$$u\frac{\partial u}{\partial x}+v\frac{\partial u}{\partial y}+w\frac{\partial u}{\partial z}=\nu\frac{\partial^2 u}{\partial z^2}-\nu'\frac{\partial^4 u}{\partial z^4}-\frac{\sigma B_o^2}{\rho_f}u-\frac{\mu}{\rho_f K}u, \tag{2}$$

$$u\frac{\partial v}{\partial x}+v\frac{\partial v}{\partial y}+w\frac{\partial v}{\partial z}=\nu\frac{\partial^2 v}{\partial z^2}-\nu'\frac{\partial^4 v}{\partial z^4}-\frac{\sigma B_o^2}{\rho_f}v-\frac{\mu}{\rho_f K}v, \tag{3}$$

$$u\frac{\partial T}{\partial x}+v\frac{\partial T}{\partial y}+w\frac{\partial T}{\partial z}=\alpha\frac{\partial^2 T}{\partial z^2}-\frac{1}{(\rho c)_f}\frac{\partial q_r}{\partial z}+\frac{Q(T-T_\infty)}{(\rho c)_f}+\frac{(\rho c)_p}{(\rho c)_f}\begin{pmatrix}D_B\left(\frac{\partial T}{\partial z}\frac{\partial C}{\partial z}\right)\\+\frac{D_T}{T_\infty}\left(\frac{\partial T}{\partial z}\right)^2\end{pmatrix}, \tag{4}$$

$$u\frac{\partial C}{\partial x}+v\frac{\partial C}{\partial y}+w\frac{\partial C}{\partial z}=D_B\left(\frac{\partial^2 C}{\partial z^2}\right)+\frac{D_T}{T_\infty}\left(\frac{\partial^2 T}{\partial z^2}\right), \tag{5}$$

with the boundary conditions which can be written by as follows:

$$u=U_w(x)=ax\,,\ v=V_w(y)=by\,,\ w=0\,,T=T_w(x)\,, \tag{6}$$

$$D_B \frac{\partial C}{\partial z} + \frac{D_T}{T_\infty}\frac{\partial T}{\partial z} = 0, \quad at \quad z = 0,$$
$$u \to 0\,, v \to 0\,, T \to T_\infty, \quad C \to C_\infty, \ at \quad z \to \infty, \tag{7}$$

where $u\,, v$ and w represent the velocity components in the $x-$, $y-$ and $z-$ directions respectively, $\nu = \mu/\rho_f$ is the kinematic viscosity, μ is the dynamic viscosity, K is the permeability, ρ_f is the density of base fluid, $\nu' = n/\rho_f$ is the couple stress viscosity, n is the couple stress viscosity parameter, σ is the electrical conductivity, T is the temperature, $\alpha = k/(\rho c)_f$ is the thermal diffusivity of base fluid, k is the thermal conductivity, $(\rho c)_f$ is the heat capacity of fluid, q_r is the nonlinear radiative heat flux, $(\rho c)_p$ is the effective heat capacity of nanoparticles, D_B is the Brownian diffusion coefficient, C is the nanoparticles concentration, D_T is the thermophoretic diffusion coefficient, T_w and T_∞ are the temperatures of the surface and far away from the surface and C_∞ is the nanoparticles concentration far away from the surface, not that *w* denotes the wall condition.
The velocities of the stretching surface and the wall temperature are:

$$U_w(x) = ax\,, V_w(y) = by\,, T_w(x) = T_\infty + T_o x. \tag{8}$$

Where $a\,, b$ are the stretching rate and T_o refers to the initial temperature. The nonlinear radiative heat flux q_r can be written as follows:

$$q_r = -\frac{4\sigma^*}{3k^*}\frac{\partial}{\partial z}(T^4) = -\frac{16\sigma^*}{3k^*}\left(T^3 \frac{\partial T}{\partial z}\right), \tag{9}$$

$$\therefore \frac{1}{(\rho c)_f}\frac{\partial q_r}{\partial z} = \frac{1}{(\rho c)_f}\frac{\partial}{\partial z}\left(-\frac{4\sigma^*}{3k^*}\frac{\partial T^4}{\partial z}\right) = -\frac{16\sigma^*}{3k^*(\rho c)_f}\frac{\partial}{\partial z}\left(T^3 \frac{\partial T}{\partial z}\right). \tag{10}$$

When substituting by equation (10) in equation (4) the energy equation takes the following form:

$$u\frac{\partial T}{\partial x} + v\frac{\partial T}{\partial y} + w\frac{\partial T}{\partial z} = \alpha\frac{\partial^2 T}{\partial z^2} - \frac{16\sigma^*}{3k^*(\rho c)_f}\frac{\partial}{\partial z}\left(T^3 \frac{\partial T}{\partial z}\right) + \frac{Q(T-T_\infty)}{(\rho c)_f} + \frac{(\rho c)_p}{(\rho c)_f}\begin{pmatrix} D_B\left(\frac{\partial T}{\partial z}\frac{\partial C}{\partial z}\right) \\ + \frac{D_T}{T_\infty}\left(\frac{\partial T}{\partial z}\right)^2 \end{pmatrix} \tag{11}$$

Where σ^* is the Stefan-Boltzmann constant and k^* is the mean absorption coefficient. The similarity transformations and nondimensional variables used to convert the system of governing nonlinear partial differential equations (2), (3), (5) and (11) with the boundary conditions (6) and (7) are given in the following mathematical formulas:

$$u = axf'(\eta), v = byg'(\eta), w = -\sqrt{a\nu}\big(f(\eta) + g(\eta)\big),$$
$$\theta(\eta) = \frac{T-T_\infty}{T_w-T_\infty}, \phi(\eta) = \frac{C}{C_\infty}, \eta = \sqrt{\frac{a}{\nu}}z. \tag{12}$$

It can be using the temperature ratio parameter

$$\theta_W = \frac{T_w}{T_\infty} \Rightarrow T = T_\infty(1 + (\theta_W - 1)\theta), T_W > T_\infty\,.$$

Now the continuity equation (1) was automatically satisfied and the governing nonlinear partial differential equations (2), (3), (5) and (11) were converted by using the similarity transformations and nondimensional variables (12) to a new system of nonlinear ordinary differential equations as follows:

$$f'''(\eta) + \big(f(\eta) + g(\eta)\big)f''(\eta) - \big(f'(\eta)\big)^2 - K_s f'''''(\eta) - (M + Da)f'(\eta) = 0, \tag{13}$$

$$g'''(\eta) + \big(f(\eta) + g(\eta)\big)g''(\eta) - \big(g'(\eta)\big)^2 - K_s g'''''(\eta) - (M + Da)g'(\eta) = 0, \tag{14}$$

$$\theta''(\eta) + pr\Big[\big(R(1 + (\theta_w - 1)\theta)^3\theta'(\eta)\big)' + \big(f(\eta) + g(\eta)\theta'(\eta) + Nb\theta'(\eta)\phi'(\eta) + Nt\big(\theta'(\eta)\big)^2 + S\theta(\eta)\Big] = 0, \tag{15}$$

$$\phi''(\eta) + Le\big(f(\eta) + g(\eta)\big)\phi'(\eta) + \frac{Nt}{Nb}\theta''(\eta) = 0. \tag{16}$$

And the new boundary conditions can be written as follows;

$$f(0) = 0, g(0) = 0, f'(0) = 1, g'(0) = C_s, f''(0) = 0, g''(\eta) = 0, \theta(0) = 1, Nb\phi'(0) + Nt\theta'(0) = 0, \tag{17}$$

$$f'(\infty) \to 0, g'(\infty) \to 0, \quad f''(\infty) \to 0, g''(\infty) \to 0, \theta(\infty) \to 0, \phi(\infty) \to 0. \tag{18}$$

Whereas $M = \sigma {B_0}^2/\rho_f a$ is the magnetic field parameter, $K_s = \nu' a/\nu^2$ is the couple stress parameter, $C_s = b/a$ is the ratio of stretching rates, $R = 16\sigma^* T_\infty^3/3kk^*$ is the nonlinear thermal radiation parameter, $Pr = \nu/\alpha$ is the Prandtl number, $Nb = (\rho c)_p D_B C_\infty/(\rho c)_f \nu$ is the Brownian motion parameter, $Nt = (\rho c)_p D_T (T_w - T_\infty)/(\rho c)_f \nu T_\infty$ is the thermophoresis parameter, $Le = \nu/D_B$ is the Lewis number parameter, $Da = \mu/\rho_f ak$ is the Darcy number and $S = Q_o/(\rho a)_f c_p$ is the heat source $(S > 0)$ or sink $(S < 0)$ parameter.
The skin fraction coefficients and the local Nusselt number are given as follows:

$$\sqrt{Re_x}\, C_{fx} = f''(0) - K_s f''''(0), \tag{17}$$

$$\sqrt{Re_x}\, C_{fy} = g''(0) - K_s g''''(0), \tag{18}$$

$$\frac{Nu_x}{\sqrt{Re_x}} = -\left(1 + R{\theta_w}^3\right)\theta'(0), \tag{19}$$

It should be mentioned that in the absence of porous media and heat generation/absorption effects, the relevant results obtained are reduced as the results obtained by Hayat et al. [35].

NUMERICAL SOLUTION

The numerical methods that are used to solve ordinary differential equations are considered one of the best and simplest methods that enable researchers to overcome the problems they face in solving some differential equations that contain higher differential orders. On the other hand, there are many numerical methods, including, for example, the fourth order Runge-Kutta numerical method with the shooting technique, this method depends primarily on reducing the differential order of the differential equation in order to make its solution easier, this method is distinguished from other numerical methods in that the error rate in the solution is very small, and it also has a distinctive code that solves a set of differential equations for the problem within the MATLAB program. In the current study, the system of governing nonlinear partial differential equations (2), (3), (5) and (11) that controls the flow of the couple stress nanofluid with the boundary conditions (6) and (7) were transformed into a system of ordinary differential equations (13) – (16) with the new boundary conditions (17) and (18) by using the similarity transformations and nondimensional variables (12) which satisfied the continuity equation (1) and this is firstly. Secondly, the new system of nonlinear ordinary differential equations was solved numerically by using code of fourth-order Runge-Kutta method with shooting technique (which was previously mentioned) using MATLAB program in a special way, which will be present later. Function bvp4c was used to solve these equations inside MATLAB program, as that the step size $\Delta\eta = 0.001$ is used to obtain the numerical solution with $\eta_{max} = 10$. The equations (13) −(16) in the simplest form were written as follows:

$$f'''''(\eta) = \frac{\left[f'''(\eta)+(f(\eta)+g(\eta))f''(\eta)-\left(f'(\eta)\right)^2-(M+Da)f'(\eta)\right]}{K_s} \tag{20}$$

$$g'''''(\eta) = \frac{\left[g'''(\eta)+(f(\eta)+g(\eta))g''(\eta)-\left(g'(\eta)\right)^2-(M+Da)g'(\eta)\right]}{K_s} \tag{21}$$

$$\theta''(\eta) = \frac{-Pr\begin{bmatrix}(f(\eta)+g(\eta))\theta'(\eta)+Nb\theta'(\eta)\phi'(\eta)+Nt\left(\theta'(\eta)\right)^2 \\ +S\theta(\eta)+3R\left(1+(\theta_w-1)\theta(\eta)\right)^2(\theta_w-1)\left(\theta'(\eta)\right)^2\end{bmatrix}}{\left[1+PrR\left(1+(\theta_w-1)\theta(\eta)\right)^3\right]}, \tag{22}$$

$$\phi''(\eta) = -Le[f(\eta) + g(\eta)]\phi'(\eta) - \frac{Nt}{Nb}\theta''(\eta) \tag{23}$$

The previous equations (20) – (23) were entered into MATLAB program as follows:

$$F(1) = y(2),$$
$$F(2) = y(3),$$
$$F(3) = y(4),$$
$$F(4) = y(5),$$
$$F(5) = \frac{\left(y(4)+y(3)\left(y(1)+y(6)\right)-y(2)^2-(M+Da)y(2)\right)}{K_s},$$
$$F(6) = y(7),$$
$$F(7) = y(8),$$
$$F(8) = y(9),$$
$$F(9) = y(10),$$
$$F(10) = \frac{\left(y(9)+y(8)\left(y(1)+y(6)\right)-y(7)^2-(M+Da)y(7)\right)}{K_s},$$
$$F(11) = y(12),$$
$$F(12) = \frac{-Pr\begin{bmatrix}\left(y(1)+y(6)\right)y(12)+Nby(12)y(14)+Nt\left(y(12)\right)^2 \\ +Sy(11)+3R\left(1+(\theta_w-1)y(11)\right)^2(\theta_w-1)\left(y(12)\right)^2\end{bmatrix}}{\left[1+PrR\left(1+(\theta_w-1)y(11)\right)^3\right]},$$
$$F(13) = y(14),$$
$$F(14) = -Le\left(y(1) + y(6)\right)y(14) - \frac{Nt}{Nb}F(12).$$

With the boundary conditions (6) and (7) which can be written as follows:

$$y_a(1) = 0, y_a(6) = 0, y_a(2) = 1, y_a(7) =$$

$$C_s, y_a(3) = 0, y_a(8) = 0, y_a(11) = 1,$$

$$Nby_a(14) + Nty_a(12) = 0, y_b(2) = 0, y_b(7) =$$

$$0, y_b(3) = 0, y_b(8) = 0, y_b(11) = 0,$$

$$y_b(13) = 0.$$

Taking into account all of the following:

$f(\eta) = y(9)$, $f'(\eta) = y(2)$, $f''(\eta) = y(3)$, $f'''(\eta) = y(4)$, $f''''(\eta) = y(5)$, $f'''''(\eta) = F(5)$, $g(\eta) = y(6)$, $g'(\eta) = y(7)$, $g''(\eta) = y(8)$, $g'''(\eta) = y(9)$, $g''''(\eta) = y(10)$, $g'''''(\eta) = F(10)$, $\theta(\eta) = y(11)$, $\theta'(\eta) = y(12)$, $\theta''(\eta) = F(11)$, $\phi(\eta) = y(13)$, $\phi'(\eta) = y(14)$, $\phi''(\eta) = F(14)$, $f(0) = y_a(1)$, $g(0) = y_a(6)$, $f'(0) = y_a(2)$, $g'(0) = y_a(7)$, $f''(0) = y_a(3)$, $g''(0) = y_a(8)$, $\theta(0) = y_a(11)$, $\phi'(0) = y_a(14)$, $f'(\infty) = y_b(2)$, $g'(\infty) = y_b(7)$, $f''(\infty) = y_b(3)$, $g''(\infty) = y_b(8)$, $\theta(\infty) = y_b(11)$, $\phi(\infty) = y_b(13)$.

And for the credibility of the results of the current study, a numerical comparison was made between the results of the current study and the results of the work published by Hayat et al. [49], Kandasamy at al. [53] and Ramesh at al. [54] by calculating the numerical values of the local Nusselt number $-\theta(0)$ in Tables 1, 2 and 3, it was observed that there is a strong convergence between the numerical values and this closeness in values between the previously mentioned works and the current study gives the reader or researcher great credibility for this study. As for Table 4 it shows the numerical values of the skin friction coefficients and the local Nusselt number for all the values taken by all the important physical parameters resulting from the current study.

Table 1

A comparison between the numerical values of Local Nusselt number $-\theta'(0)$ between Kandasamy et al [53], Ramesh et al. [54] and the present study for different values of Pr:

	$-\theta'(0)$		
Pr	Kandasamy et al [53]	Ramesh et al. [54]	Present study
0.7	0.4542	0.4543	0.4543
2	0.9114	0.9112	0.9091
7	0.8952	1.8953	1.8953
20	0.3538	3.3538	3.3543
70	6.4621	6.4669	6.4669

Table 2

A comparison between the numerical values of the skin friction coefficient $-Re_x^{1/2}\,C_{fx}$ for Hayat et al. [35] and the present study in in the absence each of Da and S when $R = 0.1, Nb = 0.5, Nt = 0.2, Pr = 1.2, \theta_w = 1.1, Le = 1, R = 0.1, K_s = 0.02,$

$C_s = 0.2$	Hayat et al. [49]	Present study	M = 0.1	Hayat et al. [49]	Present study
M	$-Re_x^{1/2}C_{fx}$	$-Re_x^{1/2}C_{fx}$	C_s	$-Re_x^{1/2}C_{fx}$	$-Re_x^{1/2}C_{fx}$
0.1	1.0349	1.0513	0.2	1.0349	1.0513
0.5	1.1388	1.2952	0.5	1.0899	1.0964
1	1.4114	1.5621	1	1.1724	1.0345
$C_s = 0.2$	Hayat et al. [49]	Present study	M = 0.1	Hayat et al. [49]	Present study

Table 3

A comparison between the numerical values of the skin friction coefficient $-Re_x^{1/2}\,C_{fy}$ for Hayat et al. [49] and the present study in in the absence each of Da and S when $R = 0.1, Nb = 0.5, Nt = 0.2, Pr = 1.2, \theta_w = 1.1, Le = 1, R = 0.1, K_s = 0.02,$

C_s = 0.2	Hayat et al. [49]	Present study	M = 0.1	Hayat et al. [49]	Present study
M	$-Re_x^{1/2}C_{fy}$	$-Re_x^{1/2}C_{fy}$	C_s	$-Re_x^{1/2}C_{fy}$	$-Re_x^{1/2}C_{fy}$
0.1	0.1502	0.1185	0.2	0.1502	0.1185
0.5	0.1738	0.1847	0.5	0.4676	0.4231
1	0.2462	0.2489	1	0.0455	0.0480
C_s = 0.2	Hayat et al. [49]	Present study	M = 0.1	Hayat et al. [49]	Present study

RESULTS AND DISCUSSION

As was previously explained, the flow problem of the couple stress nanofluid takes place through a suitable porous medium on an stretching sheet or a rubber surface, and the flow process is subject to some important external physical factors, which are non-linear thermal radiation, heat generation and absorption, This study resulted in an important set of physical parameters, which are; the couple stress parameter K_s, the ratio of stretching rates parameter C_s , the Brownian motion parameter Nb, the thermophoresis parameter Nt , Prandtl number Pr, Lewis number Le, the magnetic field parameter M, the Darcy number Da, the non-linear thermal radiation parameter R, the heat source/sink parameter S and the ratio temperature parameter θ_w. As for the explanation and interpretation of the results, they are presented as follows:

Velocity distribution

Figure 1 explains the effect of the magnetic field parameter M on the velocity distribution $f'(\eta)$ and by looking at this figure it can be seen that the velocity distribution decreases significantly when increasing the magnetic field parameter. Physically the increasing in the magnetic field parameter creates a counter-force to the direction of fluid this force resists the fluid's movement and its direction is counter to the fluid's movement this force is called the Lorentz force this force slows down the movement of the fluid and this is the main and sufficient physical reason for the decrease in the velocity distribution subject to the magnetic field parameter. At the same time, the effect of the Darcy number Da on the velocity distribution $f'(\eta)$ is observed in Figure 2, it explains that the velocity distribution of the fluid becomes continually decreasing when the values of the Darcy number Da enhancement. Physically, the porous medium represents one of the types of external resistance forces that work to resist the movement of the fluid through it, and thus the velocity of the fluid decreases, it is known that increasing the values of Darcy number changes the rate of fluid permeability through the porous medium, and this leads to a decrease in the velocity distribution.

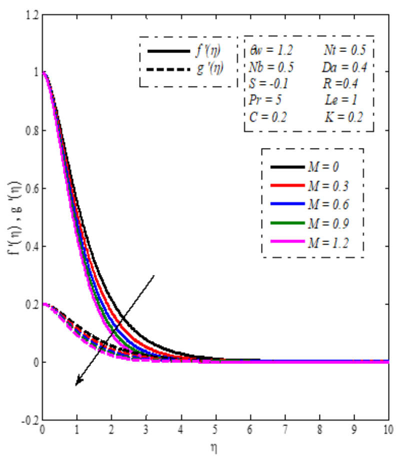

Fig. 1. Effect of the magnetic field *M* on the velocity profile.

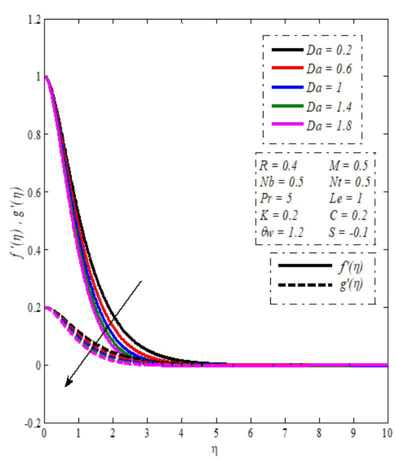

Fig. 2. Effect of Darcy number *Da* on the velocity profiles.

Temperature distributions

Figures. 3 and 4 shows the influence of non-linear thermal radiation parameter R and the ratio temperature parameter θ_w on the fluid temperature distribution $\theta(\eta)$, it is clear that the enhancement of non-linear thermal radiation parameter R and ratio temperature parameter θ_w leads to a significant rise in the fluid temperature. Physically, the enhancement in the two parameters non-linear thermal radiation parameter and the ratio temperature work to activate and reinforce the fluid particles by gaining thermal energy that increases the thermal diffusion and thermal distribution, and this in turn raises the temperature and leads to an increase in the size of the boundary layer and raising its temperature. On the other side, Prandtl number is a dimensionless quantity that puts the viscosity of the fluid in correlation with the thermal conductivity. Prandtl number is a dimensionless quantity that puts the viscosity of a fluid in correlation with the thermal conductivity. It therefore assesses the relation between momentum diffusivity and thermal diffusivity capacity of a fluid so that, Figure 5 shows the negative effect of the Prandtl number Pr on the temperature distribution $\theta(\eta)$, meaning that the greater the values of the Prandtl number, the lower the fluid temperature. Physically, the relationship between Prandtl number and temperature is invariably inverse relationship because the large Prandtl number values possess lower thermal diffusivity and the opposite is also true, thus enhancing the values of the Prandtl number make the change in the thermal diffusivity very small or it reduces the temperature distribution $\theta(\eta)$. By looking at Figure 6 you can see the change in the temperature distribution $\theta(\eta)$ under effect of the heat generation/absorption parameter S. the type ($S > 0$) means a heat generation and the type ($S < 0$) means a heat absorption, It was found that in the case of the heat generation there is an escalation in the spread and distribution of temperature $\theta(\eta)$ and also the escalation and growth of the boundary layer thickness and in the case of heat absorption this means that the temperature of the fluid becomes declining and by transporting from the heat absorption to the heat generation by enhancing the values of the heat generation/absorption parameter, a high thermal diffusion occurs that makes the temperature of the boundary layer continues to rise, and this leads to a rise in the temperature distribution of the fluid, that is the physical meaning. And when looking at the Figure 7 it can be find an enhancement in the fluid temperature distribution $\theta(\eta)$ resulted from the effect of increasing values of the thermophoresis parameter Nt on the fluid temperature distribution $\theta(\eta)$. Physically, when talking about the phenomenon thermophoresis inside the fluid, there must be two heat sources, one of which is hot that raises the temperature of the fluid around it and the other is cold, so the fluid particles from the hot source acquire a temperature that make it migrates to the cold medium, which raises the temperature of the cold medium of the fluid Therefore, the thermophoresis coefficient enhances the fluid temperature in general.

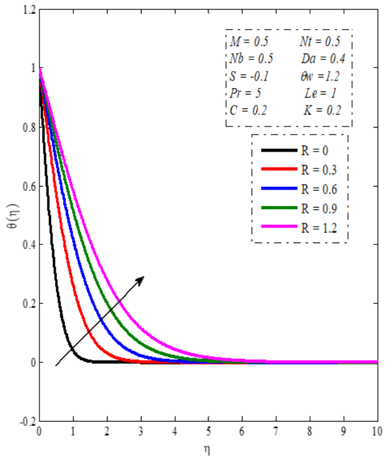

Fig. 3. Effects of nonlinear thermal radiation R on the temperature profile.

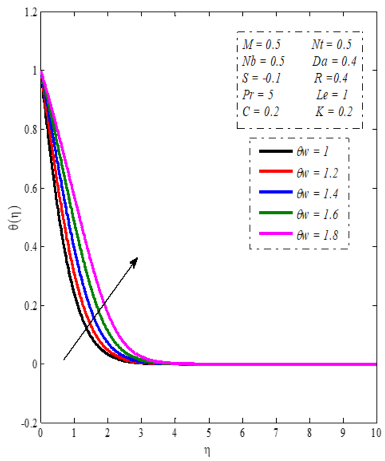

Fig. 4. Effect of the ratio temperature θ_w on the temperature profile.

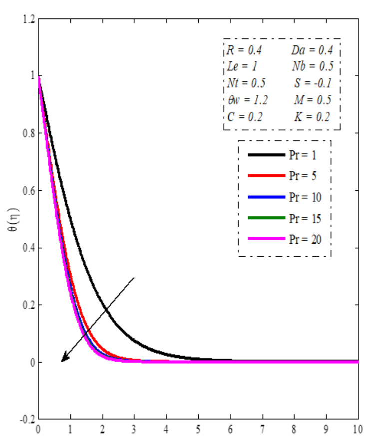

Fig. 5. Effect of Darcy number *Da* on the velocity profiles.

According to Figures 8 and 9 they illustrate the negatively impacts each of couple stress parameter K_s and the ratio of stretching rates parameter C_s on the fluid temperature distribution $\theta(\eta)$, an increase in both leads to a decrease in the thermal diffusion rate and a decrease in temperature and boundary layer size.

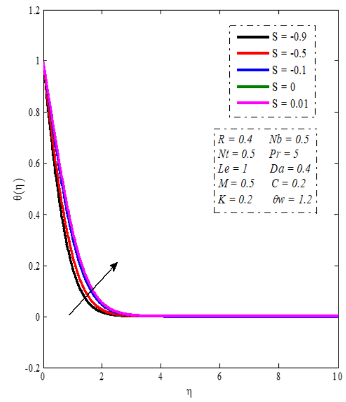

Fig. 6. Effect of the heat source/sink S on the temperature profile.

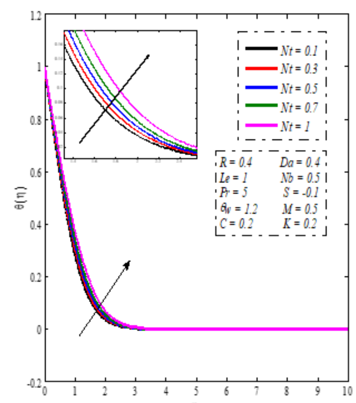

Fig. 7. Effects of the thermophoresis Nt on the temperature profile.

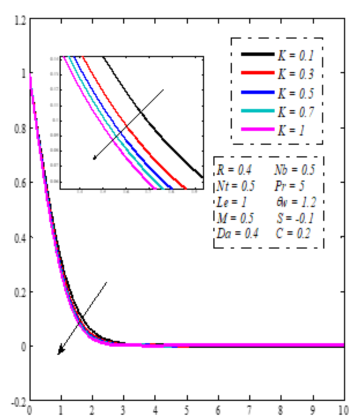

Fig. 8. Effects of couple stress parameter K_s on the temperature profile.

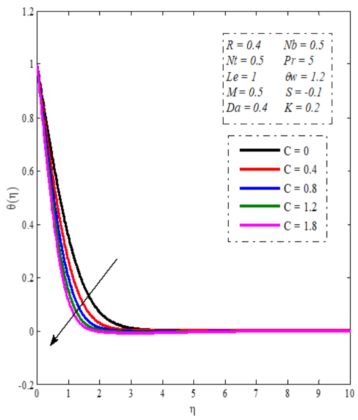

Fig. 9. Effects of parameter C_s on the temperature profile.

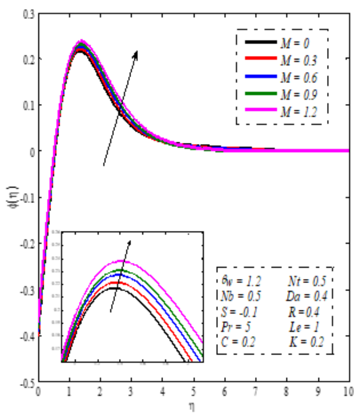

Fig. 10. Effects of magnetic field M on the concentration of nanoparticles profile.

Concentration of nanoparticles distributions

Figures 10 and 11 show the positive effects for the concentration of nanoparticles distribution under the influence of the magnetic field parameter M and Darcy number Da, the significant improvement in the concentration of nanoparticles inside the base fluid was shown when the values of the previous two parameters were enhanced. Physically, the main reason behind this is that when a magnetic field is applied to the fluid containing nanoparticles these microparticles respond to this field which stimulates them and thus increases their concentration, due to the susceptibility of these nanoparticles to their high ability to receive electric and magnetic fields see figure 10. In the case of an increase in the concentration of nanoparticles distribution when the values of Darcy number Da increase this is due to the rate of permeability of the porous medium, which makes the thickness of the boundary layer of nanoparticles continuously increasing see Figure 11. Figure 12 indicates the effect of the Brownian motion parameter Nb on the concentration of nanoparticles distribution with the remarkable improvement in the values of the Brownian motion parameter Nb a significant decrease in the concentration distribution of nanoparticles is observed within the base fluid. Physically, the improvement in the Brownian motion coefficient leads to an increase in the random movement of nanoparticles inside the fluid, which causes a decrease in the nanoparticle concentration. On the other hand, nanoparticles lose part of their kinetic energy inside the fluid which deplete the thickness of the boundary layer of nanoparticles. Regarding the change that occurs in the concentration of nanoparticles distribution in the case of the effect of the thermophoresis parameter Nt in Figure 13, it can be seen that the escalation in the values of the thermophoresis parameter leads to a higher concentration of the nanoparticle distribution. Physically, the increase in the thermophoresis parameter Nt values is followed by a rise in the thermal energy of the nanoparticles, which leads to an increase in the temperature of the liquid, and thus the nanoparticles' kinetic energy becomes very large and increases the number of collisions and this is a sufficient reason to make the distribution of the concentration of nanoparticles large under the influence of this parameter. On the other hand, Figures 14 and 15 show the large positive change in the concentration of nanoparticles distribution under the influence of the nonlinear thermal radiation parameter R and the ratio temperature parameter θ_w, it has been shown that the enhancement in the values of the nonlinear thermal radiation coefficient and the growth in the values of the temperature ratio coefficient are followed by an increase in the concentration distribution of nanoparticles. Physically, the increase in the thermal radiation coefficient and the temperature ratio values gives a very wide range of thermal diffusion within the fluid, which stimulates and increases the concentration rate of nanoparticles and also causes the growth of the boundary layer of nanoparticles thickness of due to their superior thermal conductivity. When talking about the effect of the heat source/sink parameter S on the concentration of nanoparticles distribution, you should be seeing Figure16, with the enhancement in the heat source/sink parameter S it was noted that the rate of impact becomes positive on the concentration of nanoparticles distribution. Physically when transporting from the heat sink rate to the heat source rate the nanoparticles acquire high thermal energy that increases their movement within the main fluid, which makes the rate of collisions between them large, and this leads to an increase in their concentration. Figures 17 and 18 show the negative effect of Prandtl number Pr and Lewis number Le on the concentration of nanoparticle distribution, each of them causes a weakening, reduction, and a significant decrease in this distribution. Physically, the rate of increase in Prandtl number values causes the nanoparticles to get closer to the surface and increases the chances of sticking to the surface, which makes the nanoparticle size volume weak. Brownian diffusion that makes the concentration distribution small. Finally, Figures19 and 20 shows the influence each of the ratio of stretching rates parameter C_s and the couple stress parameter K_s on the concentration of nanoparticles distribution, it was found that the enhancement in the values of these two parameters leads to a reduction in the concentration of nanoparticles distribution.

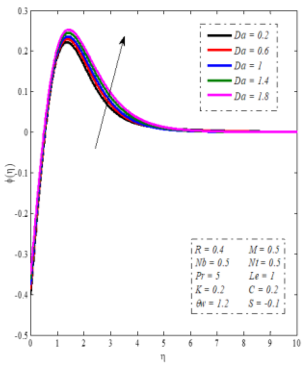

Fig. 11. Effects of the Darcy number Da on the concentration of nanoparticles profile.

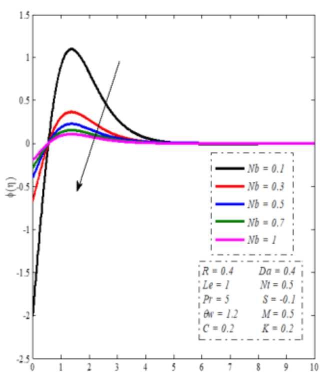

Fig. 12. Effects of the Brownian motion parameter Nb on the concentration of nanoparticles profile.

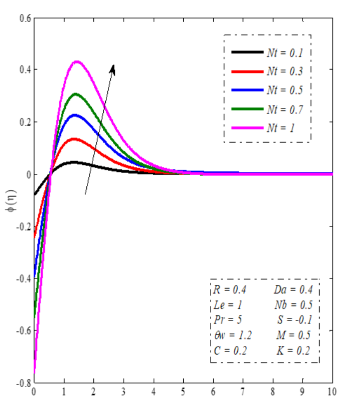

Fig. 13. Effects of the thermophoresis parameter Nt on the concentration of nanoparticles profile.

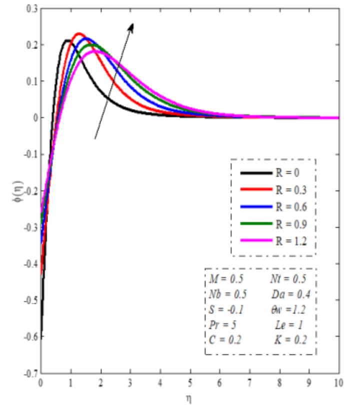

Fig. 14. Effects of the nonlinear thermal radiation parameter R on the concentration of nanoparticles profile.

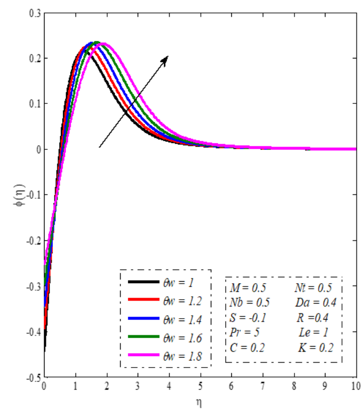

Fig. 15. Effects of the ratio radiation parameter θ_w on the concentration of nanoparticles profile.

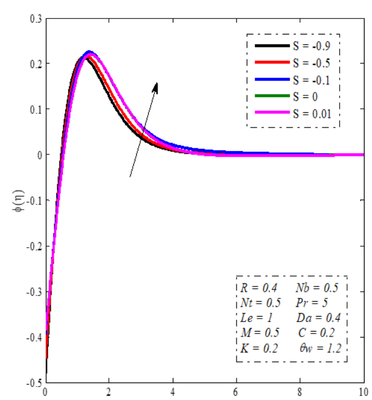

Fig. 16. Effects of the thermophoresis parameter Nt on the concentration of nanoparticles profile.

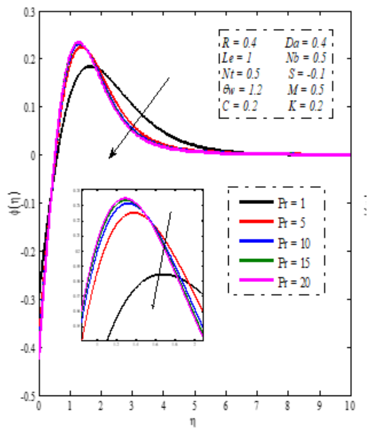

Fig. 17. Effects of the Prandtl number Pr on the concentration of nanoparticles profile.

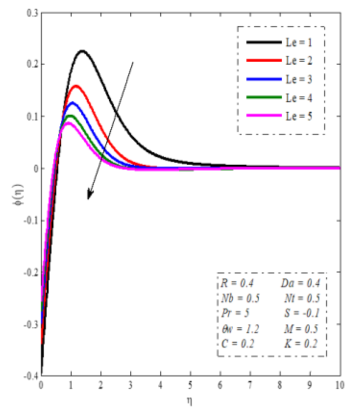

Fig. 18. Effects of the Lewis number Le on the concentration of nanoparticles profile.

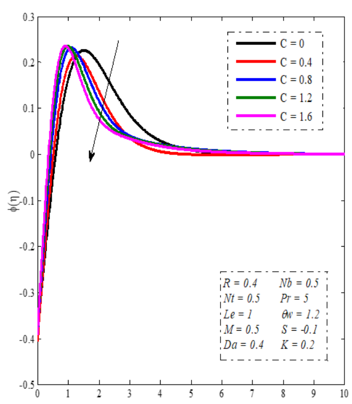

Fig. 19. Effects of the parameter C_s on the concentration of nanoparticles profile.

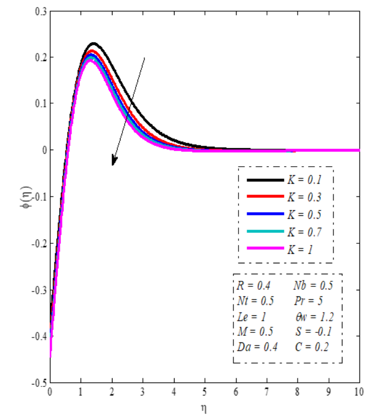

Fig. 20. Effects of the parameter K_s on the concentration of nanoparticles profile.

Profiles of the skin friction coefficient and the local Nusselt number

The Nusselt number is the ratio of convective to conductive heat transfer across a boundary. The convection and conduction heat flows are parallel to each other and to the surface normal of the boundary surface, and are all perpendicular to the mean fluid flow in the simple case. Figure 21 illustrates the influences of the heat source/sink parameter S on the local Nusselt number in presence of increase in the thermophoresis parameter Nt, it is clear that the increase in each of the previous parameters leads to the decrease in the local Nusselt number meaning that the effects are negative in the case of regular temperature gradient. The skin friction coefficient is an important dimensionless parameter in boundary layer flows, It specifies the fraction of the local dynamic pressure that is felt as shear stress on the surface so, Figures 22 and 23 shows the effects each of magnetic field parameter M and Darcy number Da on the skin friction coefficients, it has been observed that the skin friction coefficient decrease with the increasing in values of both magnetic field parameter and Darcy number, Physically, this is explained by the fact that the regular decrease in the coefficient of skin friction means the regular decrease in the velocity gradations on the surface relative to the movement of the fluid.\

CONCLUSION

The current study reviews the three-dimensional magnetohydrodynamic steady flow process of the incompressible non-Newtonian couple stress nanofluid through a suitable porous medium on a stretching surface. The flow process was subjected to some external physical factors such as non-linear thermal radiation and heat generation and absorption, taking into consideration the effect of the Brownian motion coefficient and also the effect of the thermophoresis coefficient. On the other hand, the system of nonlinear partial differential equations governing

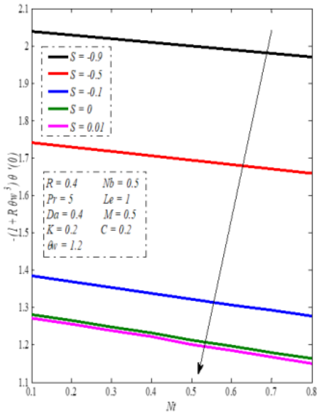

Fig. 21. Effects of the heat source/sink S and thermophoresis Nt on the local Nusselt number.

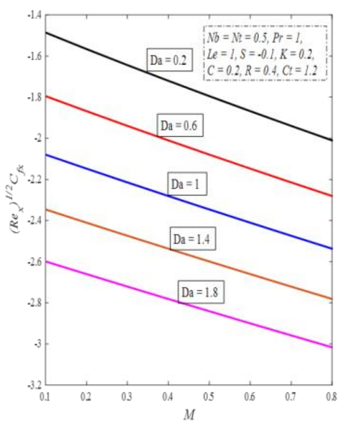

Fig. 22. Effects of the magnetic field M and the Darcy number Da on the Skin fraction $(Re_x)^{1/2}C_{fx}$.

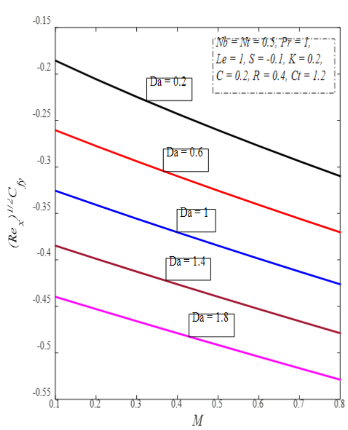

Fig. 23. Effects of the magnetic field M and the Darcy number Da on the Skin fraction $(Re_x)^{1/2}C_{fy}$.

the study of the flow problem has been transformed into a system of nonlinear ordinary differential equations by using the similarity transformations and dimensionless variables. Knowing that the new system of ordinary differential equations was solved numerically using the fourth-order Runge-Kutta method with the shooting technique using the code of the MATLAB program. The MATLAB program was used to create graphs showing the effects of all the important physical parameters resulting from the study on three main distributions that are the focus of this study, namely, the velocity distribution, the temperature distribution, and the concentration of nanoparticle distribution, in addition to, studying the effect of some of these parameters on the local Nusselt number and skin friction coefficient, with clarification of the important physical meanings of all parameters. It can be concluded the study by following remarks:

- The effects each of magnetic field parameter M and Darcy number Da were negative on the velocity distribution and positive on the concentration of nanoparticles distribution.
- The enhancement in the values of the non-linear thermal radiation parameter R, the ratio temperature parameter θ_w, the thermophoresis parameter Nt and the heat generation and absorption parameter S lead to an enhancement in the distributions of both the temperature and the concentration of nanoparticles.
- The increase in the values each of Prandtl number Pr, the couple stress parameter K_s and the ratio of stretching rates C_s leads to a decrease in the temperature distribution
- The increase in the values of Lewis number Le, Prandtl number Pr, couple stress parameter K_s, Brownian motion parameter Nb and the ratio of stretching rates C_s follow by a decrease in the concentration of nanoparticles distribution.
- The relationship between the skin friction coefficient and each of the magnetic field parameter M and the Darcy number Da is a direct negative relationship, whereas, the local Nusselt number are decreasing when enhancement each of the heat source/sink parameter S and thermophoresis parameter Nt.

ACKNOWLEDGMENT

The authors extend their appreciation to the Deanship of Scientific Research at King Khalid University for funding this work through research groups program under Grant Number (R.G.P2/27/42).

Table 4:
The values of the local Nusselt number and skin friction coefficient for Da, S, M, Ct, R, Le, Pr, Nb, K_s, C_s and Nt.

M		Da	R	Nb	Nt	K_s	C_s	Pr	Le	S	Ct	$Re_x^{-1/2}$	$Re_x^{1/2}$	$Re_x^{1/2}$
0		.4	.4	.5	.5	.2	.2	5	1	0.1	.2	4835	626	554
.3												3162	511	043
.6												1702	027	990
.5		.2	.4	.5	.5	.2	.2	5	1	0.1	.2	3162	511	043
		.6										1249	950	552
		1										9648	615	466
.5		.4	0	.5	.5	.2	.2	5	1	0.1	.2	7545	986	388
			.3									4617	986	388
			.6									1062	986	388
.5		.4	.4	.1	.5	.2	.2	5	1	0.1	.2	2246	984	388
				.3								2246	984	388
				.7								2223	990	388
.5		.4	.4	.5	.1	.2	.2	5	1	0.1	.2	8380	990	388
					.3							5299	990	388
					.7							9191	984	388
.5		.4	.4	.5	.5	.3	.2	5	1	0.1	.2	3962	168	056
						.5						6027	200	555
						.7						7293	914	477
.5		.4	.4	.5	.5	.2	0	5	1	0.1	.2	0982	186	0
							.4					2539	698	439
							.8					1182	847	283
.5		.4	.4	.5	.5	.2	.2	10	1	0.1	.2	0280	986	388
								15				3256	986	388
								20				4801	986	388
.5		.4	.4	.5	.5	.2	.2	5	2	0.1	.2	8209	984	388
									3			5632	984	388
									4			3939	978	388
.5		.4	.4	.5	.5	.2	.2	5	1	0.2	.2	2366	990	388
										0		1320	984	388
										01		0167	984	388
0.5		0.4	0.4	0.5	0.5	0.2	0.2	5	1	-0.1	.4	5895	986	388
											.6	4274	986	388
											1.8	1.25794	-1.93986	-0.29388

REFRENCES

[1] Stokes VK. Couple stresses in fluids, Phy Fluids. 1966; 9: 1710–1715.

[2] Devakar M, Sreenivasu D, Shankar B. Analytical solutions of couple stress fluid flows with slip boundary conditions, Alexandria Engineering Journal. 2014; 53: 723-730.

[3] Zhang Y, Chen X. Dielectrophoretic microfluidic device for separation of red blood cells and platelets: a model-based study, Journal of the Brazilian Society of Mechanical Sciences and Engineering. 2020; 42: 1-11.

[4] Zhang Y, Chen X. Blood cells separation microfluidic chip based on dielectrophoretic force, Journal of the Brazilian Society of Mechanical Sciences and Engineering. 2020; 42, 206.

[5] New insights into the pressure during the merged droplet formation in the squeezing time, Chemical Engineering Research and Design. 2019; 145: 213-225.

[6] Srinivasacharya D, Kaladhar K. Mixed convection flow of couple stress fluid between parallel vertical plates with Hall and Ion-slip effects, Communications in Nonlinear Science and Numerical Simulation. 2012; 17: 2447-2462.

[7] Khan NA, Khan H, Ali SA. Exact solutions for MHD flow of couple stress fluidwith heat transfer, Journal of the Egyptian Mathematical Society. 2016; 24:125-129.

[8] Ramesh K. Influence of heat and mass transfer on peristaltic flow of a couple stress fluid through porous medium in the presence of inclined magnetic field in an inclined asymmetric channel, Journal of Molecular Liquids. 2016; 219: 256-271.

[9] Adesanya SO, Souayeh B, Gorji MR, Khan MN, Adeyemi OG. Heat irreversibiility analysis for a couple stress fluid flow in an inclined channel with isothermal boundaries, Journal of the Taiwan Institute of Chemical Engineers. 2019; 101: 251-258.

[10] Choi SUS, Int. Mech. Eng. Cong. Exp. ASME, FED 231/MD. 1995; 66:99.

[11] Waqas H, Wakif A, Al-Mdallal Q, Zaydan M, Farooq U, Hussain M. Significance of magnetic field and activation energy on the features of stratified mixed radiative-convective couple-stress nanofluid flows with motile microorganisms, Alexandria Engineering Journal Available online. 2021; 8.

[12] Waseem M, Gul T, Khan I, Khan A, Saeed A, Ali I, Kumam P. Gravity-driven hydromagnetic flow of couple stress hybrid nanofluid with homogenous-heterogeneous reactions, Scientific Reports. 2021; 11.

[13] Afzal Q, Akram S, Ellahi R, Sait SM, Chaudhry F. Thermal and concentration convection in nanofluids for peristaltic flow of magneto couple stress fluid in a nonuniform channel, Journal of Thermal Analysis and Calorimetry. 2021; 144: 2203–2218.

[14] Usman M, Gul T, Khan A, Alsubie A, Ullah MZ. Electromagnetic couple stress film flow of hybrid nanofluid over an unsteady rotating disc, International Communications in Heat and Mass Transfer. 2021; 127.

[15] Narayana PVS, Tarakaramu N, Sarojamma G, Animasaun IL. Numerical simulation of nonlinear thermal radiation on the 3D flow of a couple stress Casson nanofluid due to a stretching sheet, J. Thermal Sci. Eng. Appl. 2021; 13.

[16] Tahir F, Gul T, Islam SD, Shah Z, Khan A, Khan W, Ali L, Muradullah. Flow of a Nano-Liquid Film of Maxwell Fluid with Thermal Radiation and Magneto Hydrodynamic Properties on an Unstable Stretching Sheet.J. Nanofluids. 2013; 6: 1021–1030.

[17] Naduvinamani NB, Hiremath PS, Gurubasavaraj G. Effect of surface roughness on the couple-stress squeeze film between a sphere and a flat plate, Tribology International. 2015; 38: 451-458.

[18] Biswas P, Arifuzzaman SM, Karim I, Khan MS. Impacts of magnetic field and radiation absorption on mixed convective Jeffrey nanofluid flow over a vertical stretching sheet with stability and convergence analysis.J. Nanofluids. 2017; 6: 1082–1095.

[19] Hayat T, Haider F, Muhammad T, Alsaed A. On Darcy-Forchheimer flow of viscoelastic nanofluids. Journal of Molecular Liquids. 2016; 233: 278–287.

[20] Hayat T, Qayyum S, Imtiazs M, Alsaedi A. Comparative study of silver and copper water nanofluids. International Journal of Heat and Mass Transfer. 2016; 102: 723–732.

[21] Bai Y, Liu X, Zhang Y, Zhang M. Stagnation-point heat and mass transfer of MHD Maxwell nanofluids. Journal of Molecular Liquids. 2015; 224: 1172–1180.

[22] Akbar NS, Kazmi N, Tripathi D, Mir NA. Study of heat transfer on physiological driven movement with CNT nanofluids. Computer Methods and Programs in Biomedicine. 2016; 136: 21–29.

[23] Alfvén H. Existence of electromagnetic-hydrodynamic waves. Nature. 1942; 150: 405–406.

[24] Mabood F, Yusuf TA, Bognar G. Features of entropy optimization on MHD couple stress nanofluid slip flow with melting heat transfer and nonlinear thermal radiation, Scientific Reports. 2020; 10, 19163.

[25] Ahmed SE, Mohamed RA, Aly AM, Soliman MS. Magnetohydrodynamic Maxwell nanofluids flow over a stretching surface through a porous medium: effects of non-linear thermal radiation, convective boundary conditions and heat generation/absorption, International Journal of Aerospace and Mechanical Engineering. 2019; 13: 436 – 443.

[26] Mohamed RA, Aly AM, Ahmed SE, Soliman MS, Jeffrey MHD. Nano fluids flow over a stretching sheet through a porous medium in presence of nonlinear thermal radiation and heat generation/absorption, Transport Phenomena in Nano and Micro Scales. 2020; 8: 9–22.

[27] Mohamed RA, Ahmed SE, Aly AM, Chamkha AJ, Soliman MS, MHD Casson nanofluid flow over a stretching surface embedded in a porous medium effect of thermal radiation and slop conditions, Latin American Applied Research. 2021; 51: 229-239.

[28] Bouslimi J, Omri M, Mohamed RA, Mahmoud KH, Abo-Dahab SM, Soliman MS. MHD Williamson Nanofluid Flow over a Stretching Sheet through a Porous Medium under Effects of Joule Heating, Nonlinear Thermal Radiation, Heat Generation/Absorption, and Chemical Reaction, Hindawi, Advances in Mathematical Physics, 2021.

[29] Akbar NS, Tripathi D, Khan ZH, Bégd OA. A numerical study of magnetohydrodynamic transport of nanofluids. Chemical Physics Letters. 2015; 661: 20–30.

[30] Makinde OD, Iskander T, Mabood F, Khan WA, Tshehla MS. MHD Couette-Poiseuille flow of variable viscosity nanofluids. Journal of Molecular Liquids. 2016; 221: 778-787.

[31] Nakharintr L, Naphon P. Magnetic field effect on the enhancement of nanofluids heat transfer. International Journal of Heat and Mass Transfer. 2017; 110: 753–759.

[32] Khan WA, Makinde OD. Non-aligned MHD stagnation point flow of variable viscosity nanofluids. International Journal of Heat and Mass Transfer. 2016; 96: 525–534.

[33] Changdar D, Soumen S. Analytical Solution of Mathematical Model of Magnetohydrodynamic Blood Nanofluid Flowing Through an Inclined Multiple Stenosed Artery. J. Nanofluids. 2017; 6: 1198–1205.

[34] Sedighi A. Steady Boundary Layer Magnetohydrodynamic Viscous Flow and Heat Transfer of Nanofluid over Stretching Sheet in Presence of Radiation and Heat Source. J. Nanofluids. 2017; 6: 1206–1214.

[35] Ashikin N, Bakar A, Bachok N, Arifin NM. Rotating Flow Over a Shrinking Sheet in Nanofluid Using Buongiorno Model and Thermophysical Properties of Nanoliquids.J. Nanofluids. 2017; 6: 1215–1226.

[36] Srinivasacharya D, Shafeeurrahman M. Entropy Generation Due to MHD Mixed Convection of Nanofluid Between Two Concentric Cylinders with Radiation and Joule Heating Effects. J. Nanofluids. 2017; 6: 1227–1237.

[37] Borty TC, Das K, Kundu PK. Analytical approach to a Jeffrey nanofluid flow towards a Stagnation point. Journal of Molecular Liquids. 2017; 229: 443–452.

[38] Raju CSK, Sandeep N, Malvandi A. Free convective heat transfer of MHD Cu-kerosene nanofluid. Acta Astronautica. 2016; 129: 419–428.

[39] Jalilpour B, Jafarmadar S, Rashidi MM, Ganji DD, Rahime R, Shotorban AB. MHD non-orthogonal stagnation point flow of a nanofluid towards a stretching surface. Ain Shams Engineering Journal. 2015; 54: 112-118.

[40] Imtiaza M, Hayata T, Alsaedi A. Flow of magneto nanofluid by a radiative exponentially stretching surface. Advanced Powder Technology. 2016; 27: 2214–2222.

[41] Awaisa M, Saleemb S, Hayatd T, Iruma S. Hydromagnetic couple-stress nanofluid flow over a moving convective wall: OHAM analysis. Acta Astronautica. 2016; 129: 271–276.

[42] Muhammad N, Nadeem S, Mustafa T. Squeezed flow of a nanofluid with Cattaneo–Christov heat and mass fluxes. Results in Physics. 2017; 7: 862-869 (2017).

[43] Khan NS, Gul T, Islam S, Khan A, Shah Z. Brownian Motion and Thermophoresis Effects on MHD Mixed Convective Thin Film Second-Grade Nanofluid Flow with Hall Effect and Heat Transfer Past a Stretching Sheet.J. Nanofluids. 2017; 6: 812–829.

[44] Reddy MG, Reddy GRS. Temperature-Dependent Viscosity and Second Order Slip Flow on MHD Casson Radiative Nanofluid Over Stretching Sheet.J. Nanofluids. 2017; 6: 830–839.

[45] Hussain SM, Sharma R, Mishra MK, Seth GS. Radiative Magneto-Nanofluid Over an Accelerated Moving Ramped Temperature Plate with Hall Effects.J. Nanofluids. 2017; 6: 840–851.

[46] Naramgari S, Sulochana C . MHD flow of dusty nanofluid over a stretching surface. Ain Shams Engineering Journal. 2016; 7: 709-716.

[47] Mhanthesha B, Gireesha BJ, Gorlac RSR. Nonlinear radiative heat transfer in MHD three-dimensional flow. Journal of the Nigerian Mathematical Society. 2016; 35: 178-198.

[48] Kumar RVMSSK, Varma SVK. Hydromagnetic Boundary Layer Slip Flow of Nanofluid Through Porous Medium Over a Slendering Stretching Sheet.J. Nanofluids 6: 852–861.
[49] Hayat T, Muhammad T, Alsaedi A, Alhuthali MS. magnetohydrodynamic three-dimensional flow of viscoelastic nanofluid in presence of nonlinear thermal radiation, Journal of Magnetism and Magnetic Material. 2015; 385: 222-229.
[50] Mohamed RA, Abo-Dahab SM. Influence of chemical reaction and thermal radiation on the heat and mass transfer in MHD micropolar flow over a vertical moving porous plate in a porous medium with heat generation, Int. J. Thermal Science. 2009; 48: 1800 –1813.
[51] Mohamed RA, Abo-Dahab SM, Nofal TA. Thermal radiation and MHD effects on free convective flow of a polar fluid through a porous medium in the presence of internal heat generation and chemical reaction, Math. Prob. Eng, 2010; 1-27.
[52] Dahab SM, Abdelhafez MA, Mebarek-Oudina F, Bilal SM. MHD casson Nanofluid flow over non-linearly heated porous medium in presence of extending surface effect with suction/injection, accepted for publication in Indian Journal of Physics.2020.
[53] Kandasamy R, Muhaimin I, Mohamad R. Thermophoresis and Brownian motion effects on MHD boundary-layer flow of a Nanofluid in the presence of thermal stratification due to solar radiation. J. Mechanical Sciences. 2013; 70: 146-154.
[54] Ramesh GK, Gireesha BJ, Hayat T, Alsaedi A. MHD flow of Maxwell fluid over a stretching sheet in the presence of nanoparticles, thermal radiation and chemical reaction. J. Nanofluids. 2015; 4: 100106.